

Thawing quintessence from the inflationary epoch to today

Gaveshna Gupta,^{1,*} Raghavan Rangarajan,^{1,†} and Anjan A. Sen^{2,‡}

¹Physical Research Laboratory, Navrangpura, Ahmedabad, 380009, India

²Centre for Theoretical Physics, Jamia Millia Islamia, New Delhi 110025, India

(Dated: August 30, 2021)

Using the latest observational data we obtain a lower bound on the initial value of the quintessence field in thawing quintessence models of dark energy. For potentials of the form $V(\phi) \sim \phi^{\pm 2}$ we find that the initial value $|\phi_i| > 7 \times 10^{18}$ GeV. We then relate ϕ_i to the duration of inflation by assuming that the initial value of the quintessence field is determined by quantum fluctuations of the quintessence field during inflation. From the lower bound on ϕ_i we obtain a lower bound on the number of e-foldings of inflation, namely, $N > 2 \times 10^{11}$. We obtain similar bounds for other power law potentials for which too we obtain $|\phi_i| > O(M_P)$.

PACS numbers: 95.36.+x, 98.80.Cq

I. INTRODUCTION

Cosmological observations [1–3] of the past one and a half decades indicate that the Universe is undergoing accelerated expansion. Although a non-zero cosmological constant can explain the current acceleration of the Universe, one still has to explain why it is so small and why only at recent times it has started to dominate the energy density of the Universe [4]. These issues have motivated the exploration of alternative theories to explain the late time acceleration as due to a source of energy referred to as dark energy [5, 6]. A quintessence model is one amongst such theories where the dark energy arises from a scalar field ϕ rolling slowly down a potential.

The equation of state parameter w can be defined as the ratio of the pressure to the energy density

$$w = p/\rho. \quad (1)$$

A cosmological constant is equivalent to $w = -1$ whereas a quintessence field generates a time dependent equation of state $w(t) > -1$. Caldwell and Linder [7] showed that the quintessence models in which the scalar field rolls down its potential towards a minimum can be classified into two categories, namely *freezing* and *thawing* models, with quite different behavior. In thawing models at early times the field gets locked at a value away from the minimum of the potential due to large Hubble damping. At late times when Hubble damping diminishes, the field starts to roll down towards the minimum. These models have a value of w which begins near -1 and gradually increases with time. In freezing models the field rolls towards its potential minimum initially and slows down at late times as it comes to dominate the Universe. These models have a value of w which decreases with time. In both cases $w \approx -1$ around the present epoch. Thawing

models with a nearly flat potential provide a natural way to produce a value of w that stays close to, but not exactly equal to -1 . The field begins with $w \approx -1$ at high redshifts, and w increases only slightly by low redshifts. These models depend on initial field values (in contrast with freezing models of quintessence which depend on the shape of the potential).

In the present work we evaluate the cosmological consequences of the evolving quintessence field in the context of thawing models by considering various observational datasets and obtain plausible initial values of the scalar field ϕ_i . A lower bound on the the allowed values of ϕ_i has been previously obtained in Ref. [8]. Our current numerical analysis provides stronger constraints on ϕ_i . We further relate the initial value to quantum fluctuations of ϕ during inflation and thereby to the duration of inflation. The lower bound on ϕ_i then provides a lower bound on the number of e-foldings of inflation in our scenario where the initial value of the quintessence field is determined by quantum fluctuations of the field during inflation. Our work in this article is organised as follows. In section II we describe the thawing quintessence model in the standard minimal framework. In section III we provide a detailed description of the datasets used to obtain the observational constraints on the parameters of the model. In section IV we use the results obtained in our investigation to obtain a lower bound on the initial value of ϕ . We then discuss the generation of the initial value by quantum fluctuations during inflation and use the lower bound on ϕ_i to obtain a lower bound on the number of e-foldings of inflation, N . We end with our conclusions in section V.

II. THE THAWING QUINTESSENCE SCENARIO

We will assume that the dark energy is provided by a minimally coupled scalar field ϕ with the equation of

*Electronic address: gaveshna@prl.res.in

†Electronic address: raghavan@prl.res.in

‡Electronic address: aasen@jmi.ac.in

motion for the homogeneous component given by

$$\ddot{\phi} + 3H\dot{\phi} + \frac{dV}{d\phi} = 0, \quad (2)$$

where the Hubble parameter H is given by

$$H = \left(\frac{\dot{a}}{a}\right) = \sqrt{\rho/3M_P^2}. \quad (3)$$

Here $a(t)$ is the scale factor, ρ is the total density, and $M_P = (8\pi G)^{-1/2} = 2.4 \times 10^{18}$ GeV is the reduced Planck mass. Eq. (2) indicates that while the field rolls downhill in the potential $V(\phi)$, its motion is damped by a term proportional to H . The pressure and density of the scalar field are given by

$$p = \frac{\dot{\phi}^2}{2} - V(\phi) \quad (4)$$

and

$$\rho = \frac{\dot{\phi}^2}{2} + V(\phi) \quad (5)$$

respectively, and the equation of state parameter w is given by Eq. (1). At late times, the Universe is dominated by dark energy due to ϕ , and non-relativistic matter.¹ We assume a flat Universe so that $\Omega_\phi + \Omega_m + \Omega_r = 1$. Then Eqs. (2) and (3) can be rewritten in terms of the variables x , y , and λ defined by

$$x \equiv \phi'/(M_P\sqrt{6}), \quad (6)$$

$$y \equiv \sqrt{V(\phi)/(3H^2M_P^2)}, \quad (7)$$

$$\lambda \equiv -\frac{M_P}{V} \frac{dV}{d\phi}, \quad (8)$$

where the prime denotes the derivative with respect to $\ln a$; e.g., $\phi' \equiv a(d\phi/da)$. x^2 gives the contribution of the kinetic energy of the scalar field to Ω_ϕ , and y^2 gives the contribution of the potential energy, so that

$$\Omega_\phi = x^2 + y^2, \quad (9)$$

while the equation of state is rewritten as

$$\gamma \equiv 1 + w = \frac{2x^2}{x^2 + y^2}. \quad (10)$$

It is convenient to work in terms of γ , since we are interested in models for which w is near -1 , so γ is near zero.

¹ In our numerical analysis we will go back in time till decoupling. At that epoch the energy density in radiation will be more than that in ϕ . The radiation component Ω_r is included in our numerical analysis.

Eqs. (2) and (3), in a Universe containing only matter and a scalar field, become [9]

$$x' = -3x + \lambda\sqrt{\frac{3}{2}}y^2 + \frac{3}{2}x[1 + x^2 - y^2], \quad (11)$$

$$y' = -\lambda\sqrt{\frac{3}{2}}xy + \frac{3}{2}y[1 + x^2 - y^2], \quad (12)$$

$$\lambda' = -\sqrt{6}\lambda^2(\Gamma - 1)x, \quad (13)$$

where

$$\Gamma \equiv V \frac{d^2V}{d\phi^2} / \left(\frac{dV}{d\phi}\right)^2. \quad (14)$$

We numerically solve the system of Eqs. (11) - (13), initially for $V \sim \phi^{\pm 2}$, from an initial time t_i at decoupling till t_0 today. We choose $\gamma_i \sim 0$, and for different values of λ_i and Ω_{m0} we obtain x , y and λ as functions of a .² The information about the potential is encoded in the parameter Γ given above. We use our solutions for x and y , and the relation $a^{-1} = 1 + z$ (with $a_0 = 1$), to obtain the normalized Hubble parameter

$$\begin{aligned} \mathcal{H}^2(z, \lambda_i, \Omega_{m0}) &\equiv \frac{H^2(z, \lambda_i, \Omega_{m0})}{H_0^2} \\ &= \frac{8\pi G}{3H_0^2} (\rho_{m0}(1+z)^3 + \rho_{r0}(1+z)^4 + \rho_\phi(z, \lambda_i, \Omega_{m0})) \\ &= \Omega_{m0}(1+z)^3 + \Omega_{r0}(1+z)^4 + \Omega_\phi(z, \lambda_i, \Omega_{m0})\mathcal{H}^2 \\ &= \frac{\Omega_{m0}(1+z)^3 + \Omega_{r0}(1+z)^4}{(1 - \Omega_\phi(z, \lambda_i, \Omega_{m0}))}, \end{aligned} \quad (15)$$

where Ω_ϕ is given by Eq. (9).

We then utilise this expression of the Hubble parameter to calculate the luminosity distance and angular diameter distance and relate them and \mathcal{H} to the observations of type Ia supernovae (SN) data [10], the baryon acoustic oscillations (BAO) data [11], the cosmic microwave background (CMB) shift parameter [12] and the observational Hubble parameter (HUB) data [13] and constrain the parameter space for each model defined by the values of λ_i and Ω_{m0} . The allowed values of λ_i from our numerical analysis give constraints on ϕ_i , the value of ϕ at decoupling. We then extend our analysis to study other power law potentials, $V = A\phi^n$. Thereafter, based on our arguments below, we set $\phi_i \sim \phi_I$, where ϕ_I is the value of ϕ at the end of inflation. We then study the conditions on inflation to obtain ϕ_I .

² Our code solves Eqs. (11)-(13) for initial values x_i , y_i and λ_i , where x_i and y_i are derived using Eqs. (9) and (10) from initial values γ_i and $\Omega_{\phi i}$. We choose a small value of $\gamma_i \sim 10^{-9}$ and do not vary it for our analysis. For a certain λ_i , we choose a value of Ω_{m0} and then vary $\Omega_{\phi i}$ till we get a solution that satisfies $\Omega_{\phi 0} = 1 - \Omega_{m0} - \Omega_{r0}$. We identify this solution for x , y and λ as relevant for the chosen values of λ_i and Ω_{m0} (having swapped the variable $\Omega_{\phi i}$ with Ω_{m0}). This process is repeated for different values of λ_i and Ω_{m0} . We also set $\Omega_{r0} = 9.22 \times 10^{-5}$ from Planck [12].

III. OBSERVATIONAL DATASETS

We use the χ^2 analysis to constrain the parameters of our assumed parameterization. We will use the maximum likelihood method and obtain the total likelihood function for the parameters λ_i and Ω_{m0} in a model as the product of independent likelihood functions for each of the datasets being used. The total likelihood function is defined as

$$\mathcal{L}_{tot}(\lambda_i, \Omega_{m0}) \equiv e^{-\frac{\chi_{tot}^2(\lambda_i, \Omega_{m0})}{2}}, \quad (16)$$

where

$$\chi_{tot}^2 = \chi_{SN}^2 + \chi_{BAO}^2 + \chi_{CMB}^2 + \chi_{HUB}^2 \quad (17)$$

is associated with the four datasets mentioned above. The best fit value of parameters is obtained by minimising χ^2 with respect to λ_i and Ω_{m0} . In a two dimensional parametric space, the likelihood contours in 1σ and 2σ confidence region are given by $\Delta\chi^2 = \chi^2 - \chi_{min}^2 = 2.3$ and 6.17 respectively.

A. Type Ia Supernovae

Type Ia supernovae are very bright and can be observed at redshifts upto $z \sim 1.4$. They have nearly the same luminosity which is redshift independent and well calibrated by the light curves. Hence they are very good standard candles.

The distance modulus of each supernova is defined as

$$\mu_{th}(z) = 5 \log_{10} D_L^{th}(z) + \mu_0, \quad (18)$$

where the theoretical Hubble free luminosity distance D_L^{th} in a flat universe for a model is given by

$$D_L^{th}(z, \lambda_i, \Omega_{m0}) = H_0 d_L^{th} = (1+z) \int_0^z \frac{dz'}{\mathcal{H}(z', \lambda_i, \Omega_{m0})}. \quad (19)$$

Above, d_L^{th} is the luminosity distance, \mathcal{H} is obtained from Eq. (15), and μ_0 is the zero point offset.

We construct the χ^2 for the supernovae analysis after marginalising over the nuisance parameter μ_0 as [14]

$$\chi_{SN}^2(\lambda_i, \Omega_{m0}) = A(\lambda_i, \Omega_{m0}) - \frac{B^2(\lambda_i, \Omega_{m0})}{C}, \quad (20)$$

where

$$\begin{aligned} A(\lambda_i, \Omega_{m0}) &= \sum_i \frac{(\mu_{obs}(z_i) - \mu_{th}(z_i, \mu_0 = 0, \lambda_i, \Omega_{m0}))^2}{\sigma_{\mu_{obs}}^2(z_i)} \\ B(\lambda_i, \Omega_{m0}) &= \sum_i \frac{(\mu_{obs}(z_i) - \mu_{th}(z_i, \mu_0 = 0, \lambda_i, \Omega_{m0}))}{\sigma_{\mu_{obs}}^2(z_i)} \\ C &= \sum_i \frac{1}{\sigma_{\mu_{obs}}^2(z_i)}. \end{aligned} \quad (21)$$

(A should not be confused with the coefficient of the $V \sim \phi^{-2}$ potential.) $\mu_{obs}(z_i)$ is the observed distance modulus at a redshift z_i and $\sigma_{\mu_{obs}}(z_i)$ is the error in the measurement of $\mu_{obs}(z_i)$. The latest Union2.1 compilation [10] of supernovae Type Ia data consists of the measurement of distance moduli $\mu_{obs}(z_i)$ at 580 redshifts z_i over the range $0.015 \leq z \leq 1.414$ with corresponding $\sigma_{\mu_{obs}}(z_i)$. In our analysis we include the χ_{SN}^2 given by Eq. (20) in Eq. (17).

B. Baryon Acoustic Oscillations

Baryon acoustic oscillations (BAO) refers to oscillations at sub-horizon length scales in the photon-baryon fluid before decoupling due to collapsing baryonic matter and counteracting radiation pressure. The acoustic oscillations freeze at decoupling, and imprint their signatures on both the CMB (the acoustic peaks in the CMB angular power spectrum) and the matter distribution (the baryon acoustic oscillations in the galaxy power spectrum).

To obtain the constraints on our models from the BAO we use the comoving angular diameter distance

$$d_A^{th}(z_*, \lambda_i, \Omega_{m0}) = \frac{1}{H_0} \int_0^{z_*} dz' / \mathcal{H}(z', \lambda_i, \Omega_{m0}). \quad (22)$$

The redshift at decoupling z_* is obtained from the fitting formula in Ref. [15] as 1090.29.³ The dilation scale D_V [16] is given by

$$\begin{aligned} D_V^{th}(z_{BAO}, \lambda_i, \Omega_{m0}) &= H_0 \left(\frac{z_{BAO}}{\mathcal{H}(z_{BAO}, \lambda_i, \Omega_{m0})} \right)^{1/3} \\ &\times \left(\int_0^{z_{BAO}} \frac{dz}{\mathcal{H}(z, \lambda_i, \Omega_{m0})} \right)^{2/3} \end{aligned}$$

where $\mathcal{H}(z, \lambda_i, \Omega_{m0})$ is obtained from Eq. (15). We construct the χ^2 for the BAO analysis as

$$\chi_{BAO}^2(\lambda_i, \Omega_{m0}) = \sum_{ij} (x_i - d_i)(C_{ij})^{-1}(x_j - d_j), \quad (23)$$

where $x_i = \frac{d_A^{th}(z_*, \lambda_i, \Omega_{m0})}{D_V^{th}(z_{BAO}, \lambda_i, \Omega_{m0})}$ are the values predicted by a model, d_i is the mean value of $\left(\frac{d_A^{obs}(z_*)}{D_V^{obs}(z_{BAO})} \right)$ from observations given in Table 1 of Ref. [11], and $(C_{ij})^{-1}$ is the inverse covariance matrix in Eq. (3.24) of Ref. [11]. We include χ_{BAO}^2 in Eq. (17).

³ In calculating z_* we have used the mean values of $\Omega_{b0}h^2$ and $\Omega_{c0}h^2$ from Planck+WP [12].

C. Cosmic Microwave Background

The locations of peaks and troughs of the acoustic oscillations in the CMB angular spectra are sensitive to the distance to the decoupling epoch. To obtain the constraints from CMB we utilise the *shift parameter* R from Planck [12]. The CMB shift parameter R is given by

$$R^{th}(z_*, \lambda_i, \Omega_{m0}) \equiv \sqrt{\Omega_{m0} H_0^2} d_A^{th}(z_*, \lambda_i, \Omega_{m0}) \quad (24)$$

where $d_A^{th}(z_*, \lambda_i, \Omega_{m0})$ is given by Eq. (22).

The shift parameter $R(z_*)$ from Planck observations is 1.7499 ± 0.0088 [12]. Thus we obtain χ_{CMB}^2 as

$$\chi_{CMB}^2(\lambda_i, \Omega_{m0}) = \left(\frac{1.7499 - R^{th}(z_*, \lambda_i, \Omega_{m0})}{0.0088} \right)^2. \quad (25)$$

D. The observational Hubble parameter $H(z)$

The parameter $H(z)$ describes the expansion history of the Universe and plays a central role in connecting dark energy theories and observations. An independent approach, regarding the measurement of the expansion rate is provided by ‘cosmic clocks’. The best cosmic clocks are galaxies. The observational Hubble parameter data can be obtained based on differential ages of galaxies.

Recently, Farooq et al. have compiled a set of 28 datapoints for $H(z)$ data, listed in Table 1 of Ref. [13]. We use the measurements from Ref. [13] of the Hubble parameter $H_{obs}(z_i)$ at redshifts z_i , with corresponding one standard deviation uncertainties σ_i , and the current value of the Hubble parameter $H_0 = 67.3 \pm 1.2$ km s⁻¹Mpc⁻¹ from Planck [12]. Then for $\mathcal{H} = H/H_0$

$$\chi_{HUB}^2(\lambda_i, \Omega_{m0}) = \sum_i \left(\frac{\mathcal{H}_{obs}(z_i) - \mathcal{H}_{th}(z_i, \lambda_i, \Omega_{m0})}{\sigma_{\mathcal{H}_{obs}(z_i)}} \right)^2 \quad (26)$$

with $\mathcal{H}_{th}(z, \lambda_i, \Omega_{m0})$ obtained from Eq. (15), and $\sigma_{\mathcal{H}_{obs}}$ obtained from σ_i and the uncertainty in H_0 .

IV. RESULTS AND DISCUSSION

In Figs. 1 and 2 we present the likelihood contours after combining all the datasets for $V \sim \phi^{\pm 2}$. We find that for $V \sim \phi^2$ the values of $|\lambda_i|$ greater than 0.67 are excluded at 2σ confidence level whereas for $V \sim \phi^{-2}$ the values of $|\lambda_i|$ greater than 0.72 are excluded at 2σ confidence level. The best fit value for Ω_{m0} in both cases turns out to be 0.3003 which is within the bounds on Ω_{m0} by Planck [12]. The best fit value for λ_i is 0.0008 and 0.0009 respectively.

From Eq. (8),

$$\lambda_i = \mp \frac{2M_P}{\phi_i} \quad (27)$$

where \mp refers to $V = \frac{1}{2}m^2\phi^2, A\phi^{-2}$. For $V = \frac{1}{2}m^2\phi^2$, $|\lambda_i| < 0.67$ implies we need $|\phi_i| > 7.2 \times 10^{18}$ GeV. For $V = A\phi^{-2}$, $|\lambda_i| < 0.72$ implies we need $|\phi_i| > 6.7 \times 10^{18}$ GeV. Hereafter we take

$$|\phi_i| > 7 \times 10^{18} \text{ GeV} \quad (28)$$

for both potentials. One may obtain a similar bound for the quadratic potential by equating the energy density in ϕ today, $\rho_{\phi 0} = (1/2)m^2\phi_0^2 \approx (1/2)m^2\phi_i^2$, with $\Omega_{\phi 0} 3H_0^2/(8\pi G)$, where one has assumed that the light quintessence field has not evolved much since decoupling. Then for $\Omega_{\phi 0} = 0.7$ [12] and $m \lesssim H_0$ one gets

$$|\phi_i| \gtrsim 5 \times 10^{18} \text{ GeV}, \quad (29)$$

similar to the bound in Eq. (28). However, a priori one would not necessarily expect similar bounds. While using various observations to obtain the bound on ϕ_i in Eq. (28), we do not need to use that the mass of the quintessence field $m \leq H_0$. Given the current accuracy of observational data we obtain an upper bound on λ_i of order 1, and hence a lower bound for ϕ_i of order M_P , which agrees with the simple estimate above. However if, for example, more precise data in the future implies a smaller upper bound on λ_i then the estimate of the lower bound for ϕ_i will rise and will not match with the bound in Eq. (29). We also point out that the estimate above is only valid for a quadratic potential, while our approach is more general. Thus only an analysis as above taking into account various observations can give the relevant bounds on ϕ_i .

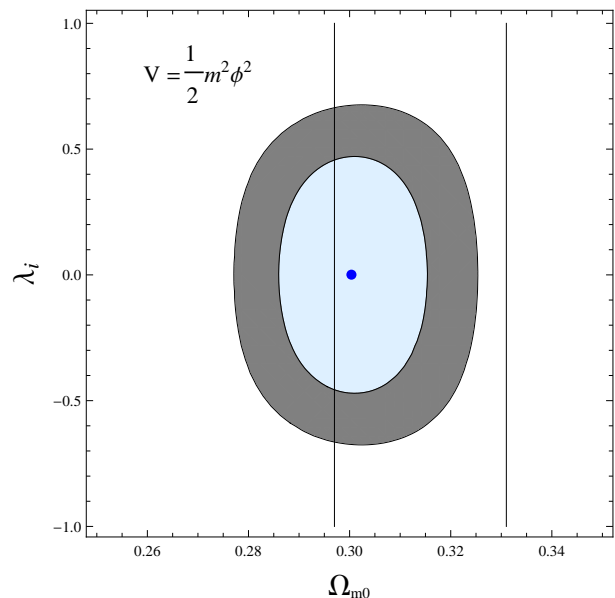


FIG. 1: The 1σ and 2σ confidence regions in the $\lambda_i - \Omega_{m0}$ plane for $V = m^2\phi^2/2$, or $\Gamma = 0.5$, constrained by the SN+BAO+CMB+HUB data. The two vertical lines represent the Planck bounds on Ω_{m0} . The thick dot represents the best fit values $\lambda_i = 0.0008, \Omega_{m0} = 0.3003$.

We note that the likelihood contours for both the potentials look very similar. This indicates that the datasets that we compare with are not able to distinguish between the different potentials under consideration. We have confirmed that the plots of x, y, λ and Ω_ϕ as functions of a , for $\Omega_{m0} = 0.3$ show variations between the potentials, but the key parameter that is relevant for comparison of the models with the different datasets is $\mathcal{H}(z)$.

In Fig. 3 we plot $\frac{\Delta\mathcal{H}_V}{\mathcal{H}}$ against z , where $\Delta\mathcal{H}_V$ is the difference in $\mathcal{H}(z)$ for the two potentials $V \sim \phi^{\pm 2}$ (the denominator corresponds to $V(\phi) \sim \phi^2$), for different values of λ_i with $\Omega_{m0} = 0.3$. The relative difference between the two potentials for $\lambda_i = 1$ reaches a maximum of about 1% and is even smaller for the other considered values of λ_i . The small relative difference is also seen in Fig. 2 of Ref. [17]. This is because in the thawing scenario the field does not roll much in its potential and hence is not sensitive to the form of the potential.

In the inset of Fig. 3 we plot $\frac{\Delta\mathcal{H}_\lambda}{\mathcal{H}}$ against z , where $\Delta\mathcal{H}_\lambda$ is the difference in $\mathcal{H}(z)$ for $\lambda_i = 1, 0.2$ for $V \sim \phi^2$ (the denominator corresponds to $\lambda_i = 0.2$), with $\Omega_{m0} = 0.3$. Though the relative difference in $\mathcal{H}(z)$ is small for different values of λ_i , the data does indicate a difference in the likelihoods for different points in the $\lambda_i - \Omega_{m0}$ plane. This is because the SN and CMB datasets disfavor large values of λ_i . The SN data has a large number of datapoints while the CMB shift parameter is very precisely measured and hence these datasets are more sensitive to the variations in λ_i .

Thus far we have presented the results for $V(\phi) \sim \phi^{\pm 2}$. In Fig. 4 we present our results for bounds on λ_i for dif-

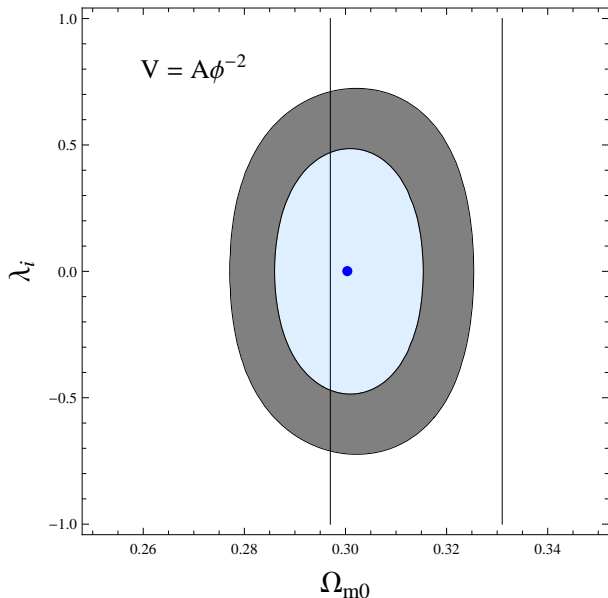


FIG. 2: The 1σ and 2σ confidence regions in the $\lambda_i - \Omega_{m0}$ plane for $V = A\phi^{-2}$, or $\Gamma = 1.5$, constrained by the SN+BAO+CMB+HUB data. The two vertical lines represent the Planck bounds on Ω_{m0} . The thick dot represents the best fit values $\lambda_i = 0.0009, \Omega_{m0} = 0.3003$.

ferent values of Γ as would be relevant for other potentials. Our analysis has been carried out for discrete values of Γ from 0 to 2, in intervals of 0.25. From Eq. (14), for potentials of the form $V = A\phi^n$, where A is taken as real and positive, $n = 1/(1 - \Gamma)$. Thus Fig. 4 includes potentials with $n = \pm 1, \pm 2, \pm 4$ for $\Gamma = 0, 2, 0.5, 1.5, 0.75, 1.25$ respectively. In addition, we have obtained the bounds for $n = \pm 3$ corresponding to $\Gamma = 2/3, 4/3$ respectively. For fractional n , the form of the potential implies ϕ has to be positive and so allowed values of $\lambda_i = -nM_P/\phi_i$ have the opposite sign of n . For integer values of n , if n is odd, positivity of the dark energy potential energy implies ϕ takes positive values. Therefore we presume that ϕ takes positive values and project the corresponding values of λ_i in Fig. 4. To simplify the numerical analysis we have taken Ω_{m0} to be 0.3. The 1σ and 2σ bound on the parameter λ_i is not very different from what we obtain in case of $V(\phi) \sim \phi^{\pm 2}$. Thus again $|\phi_i| > O(M_P)$. We mention that $\Gamma = 1$ corresponds to the case of the exponential potential $V = B \exp(\pm b\phi/\phi_i)$ and the bound on λ_i does not give a bound on ϕ_i due to the presence of the undetermined constant b .

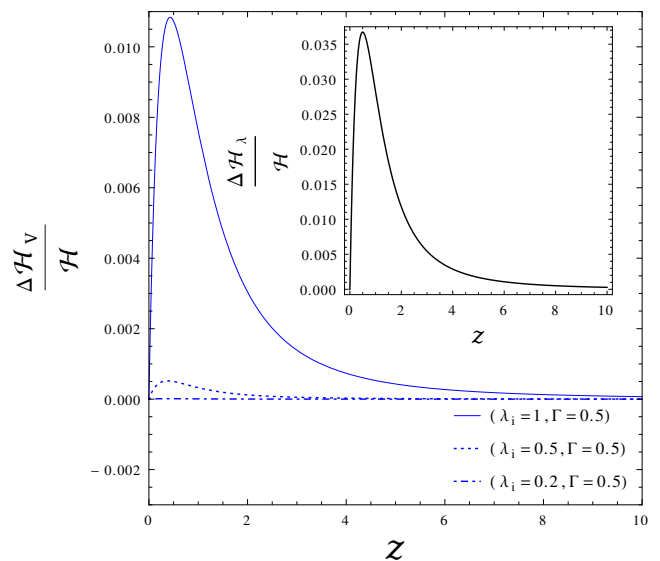


FIG. 3: The relative difference in the Hubble parameter, $\frac{\Delta\mathcal{H}_V}{\mathcal{H}}$, as a function of redshift z for $V \sim \phi^{\pm 2}$, with $\lambda_i = 0.2, 0.5$ and 1 (from bottom to top) and $\Omega_{m0} = 0.3$. The inset shows the relative difference in the Hubble parameter, $\frac{\Delta\mathcal{H}_\lambda}{\mathcal{H}}$, as a function of redshift z for $\lambda_i = 1$ and 0.2 , for $V \sim \phi^2$ and $\Omega_{m0} = 0.3$.

We now consider plausible values of ϕ_i that one may obtain in an inflationary universe by considering a condensate of ϕ being generated due to quantum fluctuations during inflation. A light scalar field of mass m ($m \ll H_I$, where H_I is the Hubble parameter during inflation) will undergo quantum fluctuations during inflation. The fluctuations are given by Eq. (7) of Ref. [18] (we presume

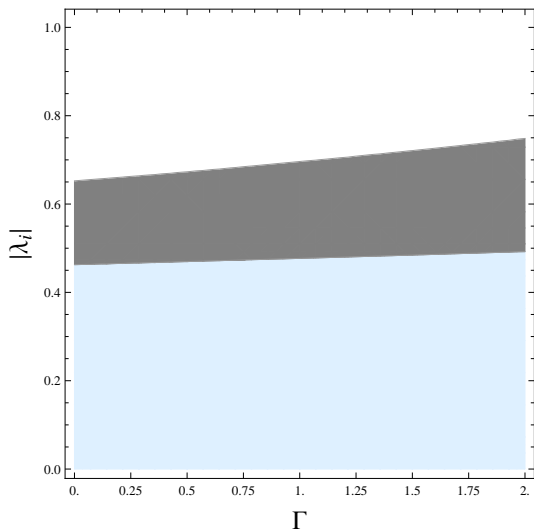


FIG. 4: The shaded region shows 1σ (blue) and 2σ (grey) confidence regions in the $|\lambda_i| - \Gamma$ plane constrained by the SN+BAO+CMB+HUB data. Discrete values for Γ in steps of 0.25 are considered here. $\Gamma = 0, 0.5, 0.75, 1.25, 1.5, 2$ corresponds to $V \sim \phi, \phi^2, \phi^4, \phi^{-4}, \phi^{-2}, \phi^{-1}$ respectively. We have taken $\Omega_{m0} = 0.3$. In addition, we have also studied Γ values of $2/3$ and $4/3$, corresponding to $V \sim \phi^{\pm 3}$.

H_I does not vary during inflation)

$$\langle \delta\phi^2 \rangle = \int_{a_i H_I}^{a H_I} \frac{d^3 k}{2\pi^3} |\delta\phi_k|^2 = \frac{3H_I^4}{8\pi^2 m^2} \left[1 - \exp\left(-\frac{2m^2 N}{3H_I^2}\right) \right] \quad (30)$$

where N is the number of e-foldings of inflation. We consider the case where $m^2 N \ll H_I^2$. Then

$$\langle \delta\phi^2 \rangle = \left(\frac{H_I}{2\pi}\right)^2 N. \quad (31)$$

Ignoring an initial value of ϕ at the beginning of inflation, and any potential driven classical evolution, the value of ϕ at the end of inflation is

$$\phi_I = \pm \sqrt{\langle \delta\phi^2 \rangle} = \pm \frac{H_I}{2\pi} \sqrt{N} \quad (32)$$

The above discussion is in the context of a quadratic potential, $V = \frac{1}{2}m^2\phi^2$. For $V = A\phi^{-2}$, and $A\phi^n$ considered in Fig. 4, we presume that the potential is very flat during inflation, and so Eq. (31) again describes the evolution of ϕ .

After inflation ϕ will evolve in two ways.

- ϕ will evolve classically in its potential $V(\phi)$. Our numerical analysis in Fig. 5 shows that the field does not evolve much between decoupling and the present epoch (less than 10 % for $|\lambda_i| < 0.7$). We expect its evolution is slower at earlier times. Therefore we may ignore the evolution of ϕ from the end of inflation till decoupling. (For a quadratic potential, $m \ll H_0 \ll H_I$ and therefore the assumption $\phi_i \sim \phi_I$ is obviously justified.)

- After inflation, modes of the ϕ field re-enter the horizon (during the radiation and matter dominated eras). These should no longer be considered part of the homogeneous ϕ condensate at late time. This can affect ϕ by removing ϕ fluctuations generated over the last 30-60 e-foldings of (electroweak to GUT scale) inflation. But our constraint on N below will be many orders of magnitude larger so we can ignore this too in our use of Eq. (32).

The above discussion implies that we may take $\phi_i \approx \phi_I$, i.e., we may assume that the field ϕ has not evolved much from inflation till decoupling. From our analysis above we have $|\phi_i| > 7 \times 10^{18} \text{ GeV}$ for $V \sim \phi^{\pm 2}$. Then, from Eq. (32), we get a lower bound on N as

$$N > \frac{2 \times 10^{39} \text{ GeV}^2}{H_I^2} \quad (33)$$

From the Planck bound on the tensor-to-scalar ratio, $H_I < 9 \times 10^{13} \text{ GeV}$ [19]. Therefore we finally obtain

$$N > 2 \times 10^{11}. \quad (34)$$

A similar bound will apply to the other power law potentials $V \sim \phi^n$.

Combining Eq. (33) and the Planck bound on H_I we get $H_I^2/N < 3 \times 10^{16} \text{ GeV}$. For a quadratic quintessence potential with $m \lesssim H_0 \approx 10^{-42} \text{ GeV}$ one sees that our assumption that $m^2 \ll H_I^2/N$ is highly feasible.

Ref. [20] also considers a dark energy condensate from quantum fluctuations of the quintessence field during inflation. Their analysis is primarily in the asymptotic limit $m^2 N \gg H_I^2$ of Eq. (30). They also consider $m^2 N \ll H_I^2$ with an argument similar to that in the paragraph following Eq. (28).

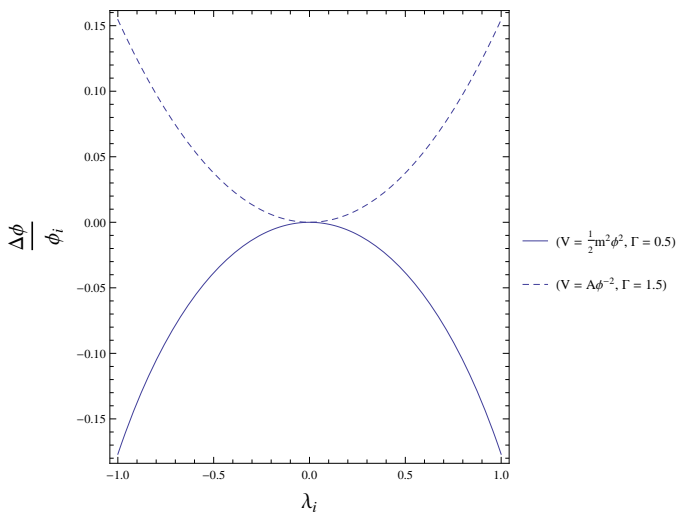


FIG. 5: The fractional change in ϕ from decoupling to today as a function of λ_i for $V = m^2\phi^2/2$ ($\Gamma = 0.5$, solid line) and $V = A\phi^{-2}$ ($\Gamma = 1.5$, dashed line). We have taken $\Omega_{m0} = 0.3$ here. For $|\lambda_i| < 0.7$, the fractional change is less than 0.1, or 10%

V. CONCLUSIONS

In this article we have first numerically solved for the evolution of the quintessence field ϕ in thawing models of dark energy for potentials of the form $V \sim \phi^{\pm 2}$ and different values of Ω_{m0} and $\lambda_i = -(M_P/V)dV/d\phi = \mp M_P/\phi_i$, where ϕ_i is the field value at decoupling. From this we obtain the Hubble parameter $H(z)$, and the luminosity distance and angular diameter distance, as given

in Eqs. (15, 19) and (22) respectively. We then relate them to the observations of type Ia supernovae data, the baryon acoustic oscillations data, the cosmic microwave background shift parameter and the observational Hubble parameter data to constrain the values of λ_i and Ω_{m0} . The likelihood contours for the two potentials looks very similar (due to similar $H(z)$ behaviour) and in both the cases we obtain $|\phi_i| > 7 \times 10^{18}$ GeV. We extend the analysis to other potentials of the form $V = A\phi^n$ and obtain the bound on the initial value of the quintessence field, assuming $\Omega_{m0} = 0.3$. Once again, we find that $|\phi_i| > O(M_P)$. We have then argued that ϕ does not evolve much between the end of inflation and decoupling and further considered a scenario where the field value at the end of inflation ϕ_I is due to quantum fluctuations of ϕ during inflation. This allows us to use the lower bound on $\phi_i \approx \phi_I$ to constrain the duration of inflation – the number of e-foldings N is constrained to be greater than 2×10^{11} , for $H_I < 9 \times 10^{13}$ GeV.

The inflationary paradigm does not stipulate an upper bound on N and so large values of N such as that required above are plausible. Large values of N are more likely in large field inflation models as discussed in Ref. [21]. However very large values of N can imply a large variation ($\gg M_P$) in the inflaton field during inflation which can be problematic if the inflationary scenario constitutes a low energy effective field theory derivable from some Planck scale theory [22]. On the other hand, one can get a large value of N in eternal inflation scenarios without a large net variation in the inflaton field [23].

Acknowledgments

RR would like to acknowledge Gaurav Goswami for useful discussions. We thank Anjishnu Sarkar for help with the plots. We thank an anonymous referee for valuable suggestions on improving this work.

-
- [1] A. G. Riess *et al.* [Supernova Search Team Collaboration], *Astron. J.* **116**, 1009 (1998) [astro-ph/9805201].
 - [2] S. Perlmutter *et al.* [Supernova Cosmology Project Collaboration], *Astrophys. J.* **517**, 565 (1999) [astro-ph/9812133].
 - [3] J. L. Tonry *et al.* [Supernova Search Team Collaboration], *Astrophys. J.* **594**, 1 (2003) [astro-ph/0305008].
 - [4] I. Zlatev, L. M. Wang and P. J. Steinhardt, *Phys. Rev. Lett.* **82**, 896 (1999) [astro-ph/9807002].
 - [5] E. J. Copeland, M. Sami and S. Tsujikawa, *Int. J. Mod. Phys. D* **15**, 1753 (2006) [hep-th/0603057].
 - [6] M. Li, X. D. Li, S. Wang and Y. Wang, *Commun. Theor. Phys.* **56**, 525 (2011) [arXiv:1103.5870].
 - [7] R. R. Caldwell and E. V. Linder, *Phys. Rev. Lett.* **95**, 141301 (2005) [astro-ph/0505494].
 - [8] G. Gupta, S. Majumdar and A. A. Sen, *Mon. Not. Roy. Astron. Soc.* **420**, 1309 (2012) [arXiv:1109.4112].
 - [9] R. J. Scherrer and A. A. Sen, *Phys. Rev. D* **77**, 083515 (2008) [arXiv:0712.3450].
 - [10] N. Suzuki, D. Rubin, C. Lidman, G. Aldering, R. Amanullah, K. Barbary, L. F. Barrientos and J. Botyanszki *et al.*, *Astrophys. J.* **746**, 85 (2012) [arXiv:1105.3470].
 - [11] R. Giostri, M. V. d. Santos, I. Waga, R. R. R. Reis, M. O. Calvao and B. L. Lago, *JCAP* **1203**, 027 (2012) [arXiv:1203.3213].
 - [12] P. A. R. Ade *et al.* [Planck Collaboration], *Astron. Astrophys.* (2014) [arXiv:1303.5076].
 - [13] O. Farooq and B. Ratra, *Astrophys. J.* **766**, L7 (2013) [arXiv:1301.5243].
 - [14] S. Nesseris and L. Perivolaropoulos, *Phys. Rev. D* **72**, 123519 (2005) [astro-ph/0511040].
 - [15] W. Hu and N. Sugiyama, *Astrophys. J.* **471**, 542 (1996) [astro-ph/9510117].
 - [16] D. J. Eisenstein *et al.* [SDSS Collaboration], *Astrophys.*

- J. **633**, 560 (2005) [astro-ph/0501171].
- [17] S. Sen, A. A. Sen and M. Sami, Phys. Lett. B **686**, 1 (2010).
- [18] A. D. Linde, Phys. Lett. B **116**, 335 (1982).
- [19] P. A. R. Ade *et al.* [Planck Collaboration], Astron. Astrophys. **571**, A22 (2014) [arXiv:1303.5082 [astro-ph.CO]].
- [20] C. Ringeval, T. Suyama, T. Takahashi, M. Yamaguchi and S. Yokoyama, Phys. Rev. Lett. **105**, 121301 (2010) [arXiv:1006.0368].
- [21] G. N. Remmen and S. M. Carroll, Phys. Rev. D **90**, 063517 (2014) [arXiv:1405.5538].
- [22] D. Baumann and L. McAllister, arXiv:1404.2601 [hep-th], see Sec. 4.3.
- [23] A. H. Guth, J. Phys. A **40**, 6811 (2007) [hep-th/0702178].